# AJNR

This information is current as of August 12, 2024.

**Normal-Appearing Cerebellar Damage in Neuromyelitis Optica Spectrum Disorder**

J. Sun, N. Zhang, Q. Wang, X. Zhang, W. Qin, L. Yang, F.-D. Shi and C. Yu

# Normal-Appearing Cerebellar Damage in Neuromyelitis Optica Spectrum Disorder

J. Sun, N. Zhang, Q. Wang, X. Zhang, W. Qin, L. Yang, F.-D. Shi, and C. Yu

## ABSTRACT

**BACKGROUND AND PURPOSE:** The cerebellum plays an important role in motor and cognitive functions. However, whether and how the normal-appearing cerebellum is impaired in patients with neuromyelitis optica spectrum disorders remain unknown. We aimed to identify the occult structural damage of the cerebellum in neuromyelitis optica spectrum disorder and its possible causes at the level of substructures.

**MATERIALS AND METHODS:** Normal-appearing gray matter volume of the cerebellar lobules and nuclei and normal-appearing white matter volume of the cerebellar peduncles were compared between patients with neuromyelitis optica spectrum disorder and healthy controls.

**RESULTS:** The cerebellar damage of patients with neuromyelitis optica spectrum disorder in the hemispheric lobule VI, vermis lobule VI, and all cerebellar nuclei and peduncles was related only to spinal lesions; and cerebellar damage in the hemispheric lobules VIII and X was related only to the aquaporin-4 antibody. The mixed cerebellar damage in the hemispheric lobules V and IX and vermis lobule Crus I was related mainly to spinal lesions; and mixed cerebellar damage in the hemispheric lobule VIIb was related mainly to the aquaporin-4 antibody. Other cerebellar substructures showed no significant cerebellar damage.

**CONCLUSIONS:** We have shown that the damage in cerebellar normal-appearing white matter and normal-appearing gray matter is associated with aquaporin-4–mediated primary damage or axonal degeneration secondary to spinal lesions or both. The etiologic classifications of substructure-specific occult cerebellar damage may facilitate developing neuroimaging markers for assessing the severity and the results of therapy of neuromyelitis optica spectrum disorder occult cerebellar damage.

**ABBREVIATIONS:** AQP4-Ab = aquaporin-4 antibody; HC = healthy control; ICP = inferior cerebellar peduncle; LSCL = length of the spinal cord lesion; MCP = middle cerebellar peduncle; NAGM = normal-appearing gray matter; NAWM = normal-appearing white matter; NMOSD = neuromyelitis optica spectrum disorder; SCI = spinal cord injury; SCN = spinal cord normal; SCP = superior cerebellar peduncle; SUIT = Spatially Unbiased Atlas Template of the Cerebellum and Brainstem

Neuromyelitis optica is an inflammatory demyelinating disorder characterized by recurrent optic neuritis and longitudinally extensive spinal cord myelitis.[1] As an expansion of neuromyelitis optica, the diagnosis of neuromyelitis optica spectrum disorder (NMOSD) also includes patients who share critical features (for example, the antibody against aquaporin-4 [AQP4-Ab]) but cannot be currently diagnosed as having neuromyelitis optica.[2] NMOSD clinical symptoms may arise from neural impairment resulting from both visible lesions and invisible pathologies on conventional MR imaging.[3]

Although many previous studies have reported structural damage in normal-appearing gray (NAGM) and white matter (NAWM) of the cerebrum in NMOSD,[4,5] our knowledge regarding damage to the cerebellum is very limited. Identifying structural damage in the normal-appearing cerebellum may improve our understanding of cerebellum-related dysfunction in NMOSD, because the cerebellum plays an important role in motor and cognitive functions.[6]

The AQP4-Ab has been identified as a highly specific serum marker[7] and plays a pathogenic role in NMOSD.[8] The cerebellum shows the highest AQP4 expression throughout the brain; thus,

the AQP4-related immune response may result in primary occult damage in the cerebellum in NMOSD. Because NMOSD-specific lesions assumed to be caused by the AQP4-related immune damage are not equally distributed in the brain, we speculated that cerebellar substructures may be unequally affected. Because there are dense connections between the spinal cord and cerebellum,[9-11] it is plausible to hypothesize that spinal lesions may result in secondary cerebellar damage via axonal degeneration in NMOSD. Considering that the connection densities between cerebellar substructures and the spinal cord are largely heterogeneous, we further hypothesized that cerebellar substructures are unequally affected. Most important, we hypothesized that we could differentiate the possible causes of the occult cerebellar damage on the basis of its association with spinal lesions and AQP4-Ab status.

In this study, we aimed not only to investigate the structural damage in NAGM and NAWM of the cerebellum in NMOSD but also to explore the possible types of normal-appearing cerebellar damage in different cerebellar substructures.

## MATERIALS AND METHODS

### Subjects
This study included 36 patients with NMOSD and 20 healthy controls (HCs). All subjects signed a written informed consent form that was approved by the Medical Research Ethics Committee of Tianjin Medical University. NMOSD was diagnosed according to the 2015 criteria.[12] Patients were excluded from the study if they met any of the following criteria: 1) beyond the range of 18–55 years of age to exclude developmental- and age-related structural changes, 2) complications from other autoimmune disorders, 3) a history of other neuropsychiatric diseases, 4) poor image quality, or 5) contraindications to MR imaging. We recorded the following information for each patient: AQP4-Ab status and brain and spinal cord MR imaging assessment. Two radiologists assessed the cerebellar lesions on brain axial T2-weighted images independently, referring to the T2-FLAIR images and excluding the subjects with visible cerebellar lesions on T2-weighted or T2-FLAIR images.[12]

### AQP4 Antibody Testing
AQP4-Ab was tested using a cell-based array through quantitative flow cytometry. For each patient with NMOSD, a serum sample was isolated from whole blood and stored in a −80°C freezer. We fixed a sample of 293 human embryonic kidney cells expressing *AQP4-M23-EGFP*-fused genes. Then we used a fluorescence microscope to detect the binding of the sera to the cells after incubation with Alexa Fluor 568-conjugated anti-human immunoglobulin G.[13]

### MR Imaging Data Acquisition
Conventional brain and spinal MRIs and brain structural imaging were acquired using a 3T MR imaging system (Discovery MR750; GE Healthcare, Milwaukee, Wisconsin). The specific imaging parameters are described in the On-line Appendix. All images were visually inspected to ensure that only images without visible artifacts were included in the subsequent analyses.

### Assessment of Spinal Cord Lesions
The length of the spinal cord lesion (LSCL) was estimated on the basis of spinal sagittal T2-weighted images by 2 radiologists independently, referring to the axial images. Interobserver agreement was assessed on the basis of weighted $\kappa$ values. The LSCL values from the 2 investigators were averaged to represent the value of each patient.

### Definition of Cerebellar Regions
The cerebellar regions were defined by the Spatially Unbiased Atlas Template of the Cerebellum and Brainstem (SUIT) (http://www.diedrichsenlab.org/imaging/suit.htm) embedded in the Statistical Parametric Mapping program (SPM12; http://www.fil.ion.ucl.ac.uk/spm). SUIT provides a high-resolution template of the human cerebellum derived from 20 healthy young individuals,[14] which preserves anatomic details of cerebellar regions using automated nonlinear normalization methods with a high accuracy in alignment among subjects.[15] SUIT provides a probabilistic atlas of cerebellar lobules and nuclei.[16] Each cerebellar hemisphere was divided into lobules I–IV, V, VI, Crus I, Crus II, VIIa, VIIIa, VIIIb, IX, and X, and the vermis was divided into lobules VI, Crus I, Crus II, VIIa, VIIIa, VIIIb, IX, and X.[6] The dentate, interposed nucleus (the combination of the globose and emboliform nuclei) and the fastigial nucleus were extracted as cerebellar nuclei. After reslicing the SUIT cerebellar template into the Montreal Neurological Institute space, we could extract cerebellar regions from the template. As the major cerebellar white matter fiber tracts connected to other parts of the CNS, the superior (SCP), middle (MCP), and inferior (ICP) cerebellar peduncles were defined by the Johns Hopkins University white-matter tractography atlas by averaging the results of deterministic tractography of 28 healthy subjects.[17]

### Calculation of Volumes of Cerebellar Regions
With SPM8, the structural images were segmented into gray matter, white matter, and CSF by a standard unified segmentation model; then, the segmented images were normalized to the Montreal Neurological Institute template by affine and nonlinear registration.[18] After inverse transformation, the transformation parameters from the Montreal Neurological Institute to native space were obtained and used to register the SUIT cerebellar subregions in Montreal Neurological Institute space to individual space. Then we could estimate the volume of each cerebellar region for each subject by counting the number of voxels in each region. To quantitatively compare NAGM volume reduction in the cerebellum, we calculated the ratio of volume reduction using the following equation: NAGM Volume Reduction Ratio = (Mean NAGM Volume of Controls − Mean NAGM Volume of NMOSD)/Mean NAGM Volume of Controls.

### Types of Normal-Appearing Cerebellar Damage
To explore the association of spinal cord lesions with cerebellar impairment in NMOSD, we divided 36 patients with NMOSD into spinal cord injury (SCI) and spinal cord normal (SCN) groups based on the presence or absence of the spinal cord lesion. Similarly, patients with NMOSD were divided into seropositive and seronegative groups based on the state of AQP4-Ab.

**Table 1: Five different types of normal-appearing cerebellar damage in NMOSD**

| Types of Occult Cerebellar Damage | SCI vs HC | | AQP4-Ab (+) vs HC | |
|---|---|---|---|---|
| | Without Controlling for AQP4-Ab Status | Controlling for AQP4-Ab Status | Without Controlling for LSCL | Controlling for LSCL |
| Type 1: only related to spinal lesions | Significant or not | Significant | Nonsignificant | Nonsignificant |
| Type 2: only related to AQP4-Ab | Nonsignificant | Nonsignificant | Significant or not | Significant |
| Type 3: mainly related to spinal lesions | Significant | Nonsignificant | Nonsignificant | Nonsignificant |
| Type 4: mainly related to AQP4-Ab | Nonsignificant | Nonsignificant | Significant | Nonsignificant |
| Type 5: no cerebellar damage | Nonsignificant | Nonsignificant | Nonsignificant | Nonsignificant |

**Note:**—+ indicates seropositive.

**Table 2: Demographics and clinical features in subjects[a]**

| | SCI | SCN | AQP4-Ab (+) | AQP4-Ab (−) | HC | $P_1$ | $P_2$ | $P_3$ | $P_4$ | $P_5$ | $P_6$ |
|---|---|---|---|---|---|---|---|---|---|---|---|
| No. | 17 | 19 | 27 | 9 | 20 | NA | NA | NA | NA | NA | NA |
| Age (yr) | 41.0 (20.5) | 41.0 (15.0) | 41.0 (12.0) | 41.0 (28.0) | 42.5 (7.5) | .297[b] | .428[b] | .827[b] | .336[b] | .390[a] | .565[b] |
| Sex (M/F) | 3:14 | 4:15 | 2:25 | 5:4 | 7:13 | .383[c] | .522[c] | .797[c] | .026[c,d] | .422[c] | .006[c,d] |
| Education (yr) | 9.0 (8.0) | 12.0 (3.0) | 12.0 (6.0) | 12.0 (3.5) | 9.0 (6.3) | .517[b] | .095[b] | .076[b] | .570[b] | .594[b] | .667[b] |
| LSCL (VS) | 3.0 (5.0) | 0.0 (0.0) | 2.0 (5.0) | 0.0 (2.5) | 0.0 (0.0) | NA | NA | NA | NA | NA | .218[b] |
| AQP4-Ab (+/−) | 15/2 | 14/5 | 27/0 | 0/9 | 0/0 | NA | NA | .271[c] | NA | NA | NA |

**Note:**—VS indicates vertebral segments; +, seropositive; −, seronegative; NA, not applicable.

[a] $P_1$: comparison between the SCI and HC groups; $P_2$: comparison between the SCN and HC groups; $P_3$: comparison between the SCI and SCN groups; $P_4$: comparison between the AQP4-Ab-seropositive and HC groups; $P_5$: comparison between the AQP4-Ab-seronegative and HC groups; $P_6$: comparison between the AQP4-Ab-seropositive and -seronegative groups. Variables are presented as median (interquartile range).

[b] The $P$ value was obtained with the Mann-Whitney $U$ test.

[c] The $P$ value was obtained with the $\chi^2$ test.

[d] Significant.

Normal-appearing cerebellar volumetric analysis was performed by the Statistical Package for the Social Sciences version 19.0 (SPSS, Chicago, IL) using General Linear Model. General Linear Model was used to compare volumetric differences in each cerebellar substructure between each pair of groups (SCI versus HC; SCN versus HC; SCI versus SCN; AQP4-Ab-seropositive versus HC; AQP4-Ab-seronegative versus HC; AQP4-Ab-seropositive versus AQP4-Ab-seronegative. All intergroup comparisons were controlled for the effects of age, sex, and educational years. The volumetric differences in cerebellar substructures between each pair of the SCI, SCN, and HC groups were also compared, further controlling for the status of AQP4-Ab. Similarly, the volumetric differences in cerebellar substructures between each pair of the AQP4-Ab seropositive, seronegative, and HC groups were also compared, further controlling for the LSCL. For exploratory analysis, an uncorrected threshold of $P < .05$ was considered significant.

According to these intergroup comparisons, the occult damage of cerebellar substructures could be categorized into 5 subtypes (Table 1)—type 1: cerebellar damage only related to spinal lesions when there was a significant difference between SCI and HC groups while controlling for the AQP4-Ab status; type 2: cerebellar damage related only to AQP4-Ab when a significant difference was found between only AQP4-seropositive and HC groups while controlling for the LSCL; type 3: mixed cerebellar damage related mainly to spinal lesions when there was a significant difference between only SCI and HC groups without controlling for the AQP4-Ab status; type 4: mixed cerebellar damage related mainly to AQP4-Ab when a significant difference was present between only AQP4-seropositive and HC groups without controlling for the LSCL; and type 5: no cerebellar damage when all comparisons were nonsignificant.

### Statistical Analyses for Demographic Variables

Statistical analyses for demographic variables were performed using the Statistical Package for the Social Sciences, Version 19.0 (IBM, Armonk, New York). Variables are presented as median (interquartile range). The Mann-Whitney $U$ test was used to detect differences in age and educational years between each pair of groups. The $\chi^2$ test was used to detect the sex differences between each pair of groups. $P < .05$ was considered statistically significant.

## RESULTS

### Demographic and Clinical Features of the Subjects

The demographic and clinical features of the subjects are summarized in Table 2. The LSCL values showed high agreement ($\kappa = 0.99$) between the 2 radiologists. There were no significant differences in age, sex, and educational years between each pair of the HC ($n = 20$), SCI ($n = 17$), and SCN ($n = 19$) groups. Although there were no significant differences in age and educational years between each pair of the HC ($n = 20$), AQP4-Ab-seropositive ($n = 27$), and AQP4-Ab-seronegative ($n = 9$) groups, the AQP4-Ab-seropositive group showed more significant female preponderance than the other 2 groups. Moreover, there were no significant differences in the presence of AQP4-Ab between the SCI and SCN groups and in the LSCL between the AQP4-Ab-seropositive and -seronegative groups.

### Group Differences in Normal-Appearing Cerebellar Volume

The NAGM and NAWM volumetric differences of cerebellar substructures between each pair of groups are shown in On-line Table 1. Volumes in normal-appearing cerebellar substructures in HC and NMOSD groups are shown in On-line Table 2. Only the SCI group showed significant cerebellar damage relative to the

HC group, without controlling for the AQP4-Ab status. Compared with the HC group, the SCI group showed a lower NAGM volume in the hemispheric lobules V (6.7% reduction, $P = .016$), VIIIa (9.5% reduction, $P = .036$), IX (16.7% reduction, $P = .036$), and X (12.8% reduction, $P = .036$); vermis lobules VI (7.6% reduction, $P = .028$) and Crus I (32.2% reduction, $P = .005$); the dentate nucleus (6.3% reduction, $P = .032$); the interposed nucleus (9.1% reduction, $P = .006$); and the fastigial nucleus (9.4% reduction, $P = .034$); and lower NAWM volume in the ICP (6.7% reduction, $P = .021$). When we further controlled for the AQP4-Ab status, compared with the HC group, the SCI group still showed lower NAGM volume in the dentate nucleus ($P = .025$), interposed nucleus ($P = .034$), and fastigial nucleus ($P = .001$) and lower NAWM volume in the ICP ($P = .026$). We additionally found a volumetric reduction in hemispheric lobule VI ($P = .048$), the SCP (8.0% reduction, $P = .034$), and MCP (3.9% reduction, $P = .040$) in the SCI group. None of the cerebellar substructures showed any significant volumetric differences between the SCN and HC groups.

The AQP4-Ab-seropositive group showed significant cerebellar impairment relative to the HC group without controlling for LSCL results. Compared with the HC group, the AQP4-Ab-seropositive group showed lower NAGM volume in hemispheric lobules VIIb (6.8% reduction, $P = .047$), VIIIa (7.4% reduction, $P = .023$), VIIIb (10.4% reduction, $P = .028$), and X (12.9% reduction, $P = .047$). When we further controlled for the LSCL, compared with the HC group, the AQP4-Ab-seropositive group still showed lower NAGM volume in the hemispheric lobules VIIIa ($P = .041$), and VIIIb ($P = .014$). We did not find volumetric reduction in the NAGM of any vermis and nuclei and in the NAWM of peduncles between the AQP4-Ab-seropositive and HC groups. None of the cerebellar substructures showed significant differences between the AQP4-Ab-seronegative and HC groups.

According to these comparisons, the occult damage of the cerebellar substructures could be categorized into 5 types—type 1: hemispheric lobule VI, vermis lobule VI, and all the cerebellar nuclei and peduncles; type 2: hemispheric lobules VIII and X; type 3: hemispheric lobules V and IX and vermis lobule Crus I; type 4: hemispheric lobule VIIb; and type 5: other cerebellar sub-structures. The distribution of each type of occult cerebellar cortical damage is shown in the Figure.

## DISCUSSION

In this study, we provided evidence for the normal-appearing cerebellar damage in NMOSD and indications for the possible causes of the observed occult damage in cerebellar substructures. The occult cerebellar damage is associated with the presence of spinal lesions or AQP4-Ab or both. The substructure-specific occult cerebellar damage and its etiologic classifications may not only help in the explanation of cerebellar dysfunction in NMOSD but may also facilitate developing neuroimaging markers for assessing etiology-specific cerebellar damage.

The volumetric reductions in several cerebellar substructures were only to hemispheric lobule VI, vermis lobule VI, and the cerebellar nuclei and peduncles, or mainly hemispheric lobules V and IX and vermis lobule Crus I associated with spinal lesions, indicating that the occult damage in these cerebellar substructures
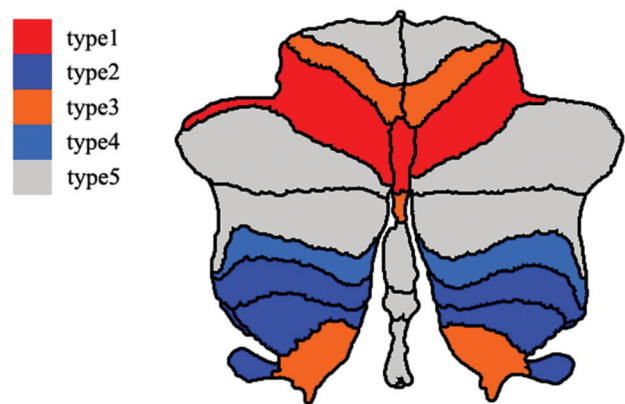


**FIGURE.** Spatial distribution of the occult cerebellar cortical damage in neuromyelitis optica spectrum disorder. Different colors represent the different types of normal-appearing cerebellar damage. Red denotes cerebellar subregions with occult damage related only to spinal lesions (type 1). Dark blue represents cerebellar subregions with occult damage related only to antibodies against aquaporin-4 antibody (type 2). Orange indicates cerebellar subregions with mixed occult damage mainly related to spinal lesions (type 3). Light blue suggests cerebellar subregions with mixed occult damage mainly related to the aquaporin-4 antibody (type 4). Gray denotes cerebellar subregions without occult damage (type 5).

is secondary to the spinal damage. There are many direct and indirect connections between spinal and cerebellar neurons. The spinocerebellar tract is the most important direct connection between spinal and cerebellar neurons and can be divided into the ventral, dorsal, and rostral spinocerebellar tracts.[9-11] These spinocerebellar tract fibers mainly project to cerebellar lobules I–V of the anterior lobe and lobules VI, VIII, and IX of the posterior lobe,[19,20] especially the lobules I–V, which play an important role in motor control via various connections.[6] Moreover, the cerebellar neurons indirectly connect with spinal neurons via a variety of nuclei in the brain stem, such as the cuneate, reticular, and inferior olivary nuclei, especially for lobules VI–VII.[21,22]

In patients with NMOSD, the spinal lesions result in damage to spinal neurons that send afferent fibers to the cerebellum. These impaired spinal neurons may lead to structural damage in the corresponding cerebellar regions via a mechanism of Wallerian degeneration through spinal-cerebellar circuitry. The axonal degeneration may better account for the NAGM reduction in these cerebellar cortices in patients with NMOSD with spinal lesions. Spinal neurons can directly connect to cerebellar nuclei, especially the interposed nucleus, via the spinocerebellar tracts and spinoreticulocerebellar tracts.[23] Moreover, the cerebellar nuclei also indirectly connect with spinal neurons via the cerebellar cortices[24] and brain stem nuclei, such as the inferior olive,[25] lateral reticular nucleus,[26] red nucleus,[27] and vestibular nuclei.[28] Based on the direct and indirect connections between the cerebellar nuclei and spinal neurons, the axonal degeneration secondary to spinal cord damage may explain why the NAGM volume of the cerebellar nuclei is reduced in NMOSD. The spinocerebellar tract fibers enter into the cerebellum directly via the SCP and ICP. More than 80% of spinocerebellar tract fibers connect with the cerebellum via the ICP, and the other spinocerebellar tract fibers link to the cerebellum via the SCP.[9-11] Moreover, most of the MCP fibers are afferent fibers from the pontine nuclei indirectly

connecting with spinal and cerebral neurons.[29] Because they are important components of the spinocerebellar and cerebropontine-cerebellar pathways, damage to the cerebellar peduncles can be explained by axonal degeneration secondary to the spinal and cerebral lesions.

The volumetric reductions in several cerebellar substructures were only to hemispheric lobules VIII and X, or mainly to hemispheric lobule VIIb, associated with the presence of AQP4-Ab, indicating that the occult damage in these cerebellar substructures is caused by AQP4-mediated immune damage. AQP4 is a transmembrane protein expressed on astrocytic end-feet surrounding blood vessels and regulates water movement among blood, brain, and CSF.[30] NMOSD is characterized by AQP4-mediated astrocyte damage,[8] the binding of AQP4 antibody to AQP4 activates complement to form membrane attack complex that leads to astrocyte injury. The resulting astrocyte injury and inflammatory reaction may further result in damage to oligodendrocytes and neurons.[31] The cerebellum has the highest AQP4 expression throughout the brain, and AQP4 is mainly rich in astrocyte cell membranes and their processes in both the granule cell and molecular layers of the cerebellum.[32,33] Furthermore, AQP4 is highly expressed in cortices near the ventricular system.[34] The posterior cerebellar lobules are located proximal to the fourth ventricle and may show a high density of AQP4.[35] Thus the AQP4-mediated astrocyte damage can be another potential cause for the structural damage of the cerebellum in NMOSD.

Clinically, patients with NMOSD frequently have cerebellar symptoms such as ataxia, tremor, and cognitive deficits.[6] Because some of these patients do not have visible cerebellar lesions on brain MR imaging, the occult damage may be the cause of these symptoms. The etiologic classifications of the occult damage in cerebellar substructures in NMOSD are clinically important. With this information, the volumes of cerebellar substructures with occult damage only or mainly caused by spinal lesions could be used to monitor the severity and the results of therapy of secondary cerebellar damage, and the volumes of cerebellar substructures with occult damage only or mainly caused by AQP4-mediated astrocyte damage could be used to monitor the severity and the results of therapy of the primary cerebellar damage in NMOSD.

Two limitations should be mentioned in this study. First, the cerebellar substructures were defined in standard space using different templates. The volumes of these substructures of each individual were calculated on the basis of the transformation parameters from the standard space to the individual space. Although advanced processing methods were used in this study, these methods may reduce interindividual volume variations. The loss of interindividual variations could influence correlation analyses between volumes of cerebellar substructures and other imaging or clinical measures. Second, our sample size was relatively small, and multiple comparisons were not corrected in this study. Thus, the results of this study should be validated in a larger sample with a more stringent statistical method.

## CONCLUSIONS

By comparing structural imaging measures of the normal-appearing cerebellum between patients with NMOSD and healthy con-

trols, we found extensive cerebellar damage in patients with NMOSD. The occult cerebellar damage is related to either spinal lesions or AQP4-Ab or both with rather heterogeneous weights. The etiology-specific occult damage in cerebellar substructures may be used to assess the severity and the results of therapy of primary and secondary cerebellar damage in NMOSD.

## REFERENCES

1. Wingerchuk DM, Lennon VA, Pittock SJ, et al. **Revised diagnostic criteria for neuromyelitis optica.** *Neurology* 2006;66:1485–89 CrossRef Medline
2. Wingerchuk DM, Lennon VA, Lucchinetti CF, et al. **The spectrum of neuromyelitis optica.** *Lancet Neurol* 2007;6:805–15 Medline
3. Wingerchuk DM, Hogancamp WF, O'Brien PC, et al. **The clinical course of neuromyelitis optica (Devic's syndrome).** *Neurology* 1999;53:1107–14 CrossRef Medline
4. Yu C, Lin F, Li K, et al. **Pathogenesis of normal-appearing white matter damage in neuromyelitis optica: diffusion-tensor MR imaging.** *Radiology* 2008;246:222–28 CrossRef Medline
5. Rocca MA, Agosta F, Mezzapesa DM, et al. **A functional MRI study of movement-associated cortical changes in patients with Devic's neuromyelitis optica.** *Neuroimage* 2004;21:1061–68 CrossRef Medline
6. Manto M, Mariën P. **Schmahmann's syndrome: identification of the third cornerstone of clinical ataxiology.** *Cerebellum Ataxias* 2015;2:2 CrossRef Medline
7. Lennon VA, Wingerchuk DM, Kryzer TJ, et al. **A serum autoantibody marker of neuromyelitis optica: distinction from multiple sclerosis.** *Lancet* 2004;364:2106–12 CrossRef Medline
8. Matiello M, Schaefer-Klein J, Sun D, et al. **Aquaporin 4 expression and tissue susceptibility to neuromyelitis optica.** *JAMA Neurol* 2013;70:1118–25 CrossRef Medline
9. Geborek P, Bengtsson F, Jörntell H. **Properties of bilateral spinocerebellar activation of cerebellar cortical neurons.** *Front Neural Circuits* 2014;8:128 CrossRef Medline
10. Cohen O, Harel R, Aumann TD, et al. **Parallel processing of internal and external feedback in the spinocerebellar system of primates.** *J Neurophysiol* 2017;118:254–66 CrossRef Medline
11. Lan CT, Wen CY, Shieh JY. **Anatomical studies on the cuneocerebellar neurons in the gerbil by using HRP method.** *Ann Anat* 1994;176:409–18 CrossRef Medline
12. Wingerchuk DM, Banwell B, Bennett JL, et al; International Panel for NMO Diagnosis. **International consensus diagnostic criteria for neuromyelitis optica spectrum disorders.** *Neurology* 2015;85:177–89 CrossRef Medline
13. Yang CS, Zhang DQ, Wang JH, et al. **Clinical features and sera anti-aquaporin 4 antibody positivity in patients with demyelinating disorders of the central nervous system from Tianjin, China.** *CNS Neurosci Ther* 2014;20:32–39 CrossRef Medline
14. Diedrichsen J. **A spatially unbiased atlas template of the human cerebellum.** *Neuroimage* 2006;33:127–38 CrossRef Medline
15. Diedrichsen J, Balsters JH, Flavell J, et al. **A probabilistic MR atlas of the human cerebellum.** *Neuroimage* 2009;46:39–46 CrossRef Medline
16. Schmahmann JD, Doyon J, McDonald D, et al. **Three-dimensional MRI atlas of the human cerebellum in proportional stereotaxic space.** *Neuroimage* 1999;10:233–60 CrossRef Medline
17. Hua K, Zhang J, Wakana S, et al. **Tract probability maps in stereotaxic spaces: analyses of white matter anatomy and tract-specific quantification.** *Neuroimage* 2008;39:336–47 CrossRef Medline
18. Ashburner J. **A fast diffeomorphic image registration algorithm.** *Neuroimage* 2007;38:95–113 CrossRef Medline
19. Sengul G, Fu Y, Yu Y, et al. **Spinal cord projections to the cerebellum**

in the mouse. *Brain Struct Funct* 2015;220:2997–3009 CrossRef Medline

20. Necker R. **Spinal neurons projecting to anterior or posterior cerebellum in the pigeon.** *Anat Embryol (Berl)* 1992;185:325–34 Medline

21. Serapide MF, Cicirata F, Sotelo C, et al. **The pontocerebellar projection: longitudinal zonal distribution of fibers from discrete regions of the pontine nuclei to vermal and parafloccular cortices in the rat.** *Brain Res* 1994;644:175–80 CrossRef Medline

22. Glickstein M, Gerrits N, Kralj-Hans I, et al. **Visual pontocerebellar projections in the macaque.** *J Comp Neurol* 1994;349:51–72 CrossRef Medline

23. Clendenin M, Ekerot CF, Oscarsson O, et al. **Functional organization of two spinocerebellar paths relayed through the lateral reticular nucleus in the cat.** *Brain Res* 1974;69:140–43 CrossRef Medline

24. Ito M, Yoshida M. **The origin of cerebral-induced inhibition of Deiters neurons, I: monosynaptic initiation of the inhibitory postsynaptic potentials.** *Exp Brain Res* 1966;2:330–49 Medline

25. Luque NR, Garrido JA, Carrillo RR, et al. **Fast convergence of learning requires plasticity between inferior olive and deep cerebellar nuclei in a manipulation task: a closed-loop robotic simulation.** *Front Comput Neurosci* 2014;8:97 CrossRef Medline

26. Wu HS, Sugihara I, Shinoda Y. **Projection patterns of single mossy fibers originating from the lateral reticular nucleus in the rat cerebellar cortex and nuclei.** *J Comp Neurol* 1999;411:97–118 CrossRef Medline

27. Hara S, Kaneyama T, Inamata Y, et al. **Interstitial branch formation within the red nucleus by deep cerebellar nuclei-derived commissural axons during target recognition.** *J Comp Neurol* 2016;524:999–1014 CrossRef Medline

28. Witter L, De Zeeuw CI, Ruigrok TJ, et al. **The cerebellar nuclei take center stage.** *Cerebellum* 2011;10:633–36 CrossRef Medline

29. Serapide MF, Zappalà A, Parenti R, et al. **Laterality of the pontocerebellar projections in the rat.** *Eur J Neurosci* 2002;15:1551–56 CrossRef Medline

30. González C, González-Buitrago JM, Izquierdo G. **Aquaporins, anti-aquaporin-4 autoantibodies and neuromyelitis optica.** *Clin Chim Acta* 2013;415:350–60 CrossRef Medline

31. Pereira WL, Reiche EM, Kallaur AP, et al. **Epidemiological, clinical, and immunological characteristics of neuromyelitis optica: a review.** *J Neurol Sci* 2015;355:7–17 CrossRef Medline

32. Hubbard JA, Hsu MS, Seldin MM, et al. **Expression of the astrocyte water channel aquaporin-4 in the mouse brain.** *ASN Neuro* 2015;7 CrossRef Medline

33. Neely JD, Amiry-Moghaddam M, Ottersen OP, et al. **Syntrophin-dependent expression and localization of aquaporin-4 water channel protein.** *Proc Natl Acad Sci U S A* 2001;98:14108–13 CrossRef Medline

34. Bradl M, Misu T, Takahashi T, et al. **Neuromyelitis optica: pathogenicity of patient immunoglobulin in vivo.** *Ann Neurol* 2009;66:630–43 CrossRef Medline

35. Amiry-Moghaddam M, Ottersen OP. **The molecular basis of water transport in the brain.** *Nat Rev Neurosci* 2003;4:991–1001 CrossRef Medline